Effect of Side Chain Length Variation on the Optical Properties of PPE-PPV Hybrid Polymers

Emine Tekin,[†] Daniel A. M. Egbe,*[,‡,†] Johannes M. Kranenburg,[†] Christoph Ulbricht, Silke Rathgeber,[§] Eckhard Birckner,[||] Nina Rehmann,[⊥] Klaus Meerholz,[⊥] and Ulrich S. Schubert*[,†,#]

Laboratory of Macromolecular Chemistry and Nanoscience, Eindhoven University of Technology and Dutch Polymer Institute (DPI), PO Box 513, 5600 MB Eindhoven, The Netherlands, Max-Planck-Institut für Polymerforschung, Polymer Physik, Ackermannweg 10, 55128 Mainz, Germany, Institut für Physikalische Chemie and Laboratory of Organic and Macromolecular Chemistry, Friedrich-Schiller Universität Jena, Lessingstrasse 10, 07743 Jena, Germany, and Institut für Physikalische Chemie, Universität Köln, Luxemburgerstrasse 116, 50939 Köln, Germany

Received November 21, 2007. Revised Manuscript Received January 25, 2008

New 4-fold alkoxy-substituted poly(*p*-phenylene-ethynylene)-*alt*-poly(*p*-phenylene-vinylene) polymers (PPE-PPV) have been synthesized in order to elucidate the previously observed effect of side chains on the thin film properties (i.e., color variation) of PPE-PPVs. The length of the side chains attached to the PPE segments, C_nH_{2n+1}, has been varied from $n = 12$ to 19. The side chains attached to the PPV segments have been kept fixed to C_8H_{17}. Polymers with $n < 16$ are yellow in color, whereas those with $n \geq 16$ are orange. Differential scanning calorimetry and nanoindentation analyses reveal side chain crystallization above room temperature in samples with longer side chains ($n \geq 16$). Reorganization of the longer side chains attached to the PPE units seems to support stronger $\pi-\pi$ overlap between the chain backbones. The red shift for $n \geq 16$ was confirmed by photoluminescence (PL) and electroluminescence (EL) spectra obtained for inkjet printed and spin-coated thin films. However, the obtained orange-red EL emission colors are unstable upon increase of the applied voltage. A blue shift of up to 100 nm was observed. All the polymers exhibited very high relative and absolute PL quantum yields in solution (~70%). Their solid-state absolute PL quantum yield was found to be between 10 and 20%. Polymeric light emitting diodes (PLED) with the following structure ITO//PEDOT:PSS//**P*n*/8**//Ca//Ag were fabricated. The devices were fully characterized and showed low turn-on voltages.

Introduction

Since the initial discovery of electrical conductivity in doped polyacetylene by Shirakawa et al.[1–3] the interest in the design, synthesis, and detailed characterization of π-conjugated polymers has grown enormously.[4,5] The solubility of the polymers has been achieved by introducing flexible alkyl and/or alkoxy side groups in poly(*p*-phenylene-vinylene)s,[6–8] poly(*p*-phenylene)s,[9–14] poly(*p*-phenylene-ethynylene)s,[15–19] and polythiophenes.[20–23] Alkoxy side chains, attached to the backbone of conjugated polymers, enhance their solubility and thus their processability into thin films by spin-coating

* To whom correspondence should be addressed. E-mail: daniel-ayuk-mbi.egbe@mb.tu-chemnitz.de (D.A.M.E); U.S.Schubert@tue.nl (U.S.S.).
† Eindhoven University of Technology and Dutch Polymer Institute.
‡ Current address: Institute of Print and Media Technology, Chemnitz University of Technology, Reichenhainer-Str. 70, D-09126 Chemnitz, Germany.
§ Max-Planck-Institut für Polymerforschung.
|| Institut für Physikalische Chemie, Friedrich-Schiller Universität Jena.
⊥ Universität Köln.
Laboratory of Organic and Macromolecular Chemistry, Friedrich-Schiller Universität Jena.

(1) Shirakawa, H.; Louis, E. J.; MacDiarmid, A. G.; Chiang, C. K.; Heeger, A. J. *J. Chem. Soc., Chem. Commun.* **1977**, 578.
(2) Chiang, C. K.; Fischer, C. R.; Park, Y. W.; Heeger, A. J.; Shirakawa, H.; Louis, E. J.; Gau, S. C.; MacDiarmid, A. G. *Phys. Rev. Lett.* **1977**, *39*, 1098.
(3) Chiang, C. K.; Druy, M. A.; Gau, S. C.; Heeger, A. J.; Louis, E. J.; MacDiarmid, A. G.; Park, Y. W.; Shirakawa, H. *J. Am. Chem. Soc.* **1978**, *100*, 1013.
(4) Skotheim, T. J.; Elsenbaumer, R. L.; Reynolds, J. R. Eds. *Handbook of Conducting Polymers*, 2nd ed.; Marcel Dekker: New York, 1998.
(5) Hadziioannou, G.; Malliaras, G. G. Eds. *Semiconducting Polymers: Chemistry, Physics and Engineering*, 2nd ed.; Wiley-VCH: Weinheim, Germany, 2007.
(6) Braun, D.; Heeger, A. J. *Appl. Phys. Lett.* **1991**, *58*, 1982.
(7) Doi, S.; Kuwabara, M.; Noguchi, T.; Ohnishi, T. *Synth. Met.* **1993**, *57*, 4174.
(8) Pfeiffer, S.; Hörhold, H.-H. *Macromol. Chem. Phys.* **1999**, *200*, 1870.
(9) Rehahn, M.; Schlüter, A.-D.; Wegner, G.; Feast, W. J. *Polymer* **1989**, *30*, 1054.
(10) Rehahn, M.; Schlüter, A.-D.; Wegner, G.; Feast, W. J. *Polymer* **1989**, *30*, 1060.
(11) Vahlenkamp, T.; Wegner, G. *Macromol. Chem. Phys.* **1994**, *195*, 8350.
(12) Karakaya, B.; Claussen, W.; Gessler, K.; Saenger, W.; Schlüter, A.-D. *J. Am. Chem. Soc.* **1997**, *119*, 3296.
(13) Kreyenschmidt, M.; Uckert, F.; Müllen, K. *Macromolecules* **1995**, *28*, 4577.
(14) Scherf, U.; Müllen, K. *Makromol. Chem., Rapid Commun.* **1991**, *12*, 489.
(15) Giesa, R.; Schulz, R. C. *Makromol. Chem.* **1991**, *191*, 857.
(16) Halkyard, C. E.; Rampey, M. E.; Kloppenburg, L.; Studer-Martinez, S. L.; Bunz, U. H. F. *Macromolecules* **1998**, *31*, 8655.
(17) Bunz, U. H. F. *Chem. Rev.* **2000**, *100*, 1605.
(18) Weder, C.; Wrighton, M. S. *Macromolecules* **1996**, *29*, 5157.
(19) Moroni, M.; Le Moigne, M.; Pham, T. A.; Bigot, J.-Y *Macromolecules* **1997**, *30*, 1964.
(20) Sato, M.; Morii, H. *Polym. Commun.* **1991**, *32*, 42.
(21) Sato, M.; Morii, H. *Macromolecules* **1991**, *24*, 1196.
(22) McCullough, R. D.; Lowe, R. D.; Jayaraman, M.; Anderson, D. L. *J. Org. Chem.* **1993**, *58*, 904.
(23) Chen, T.-A.; Wu, X.; Rieke, R. D. *J. Am. Chem. Soc.* **1995**, *117*, 233.

10.1021/cm703312u CCC: $40.75
Published on Web 03/28/2008

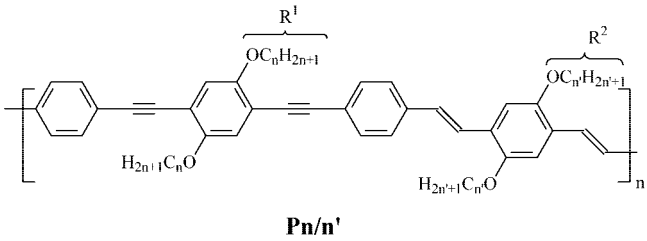

Figure 1. Chemical structure of the 4-fold alkoxy-substituted PPE-PPV polymers.

and inkjet printing. Solution processing by inkjet printing offers a low-cost, flexible and highly controlled deposition route for thin film production. Inkjet printing is in particular gaining more and more interest in the manufacturing of plastic electronics and polymer light emitting diodes (PLEDs) as well as in plastic solar cells.[24–27] Another advantage is the applicability in combinatorial material research. It enables preparation of arrays and libraries of thin films with a systematic variation such as chemical composition or thickness.[28–30] Recently, we have shown the applicability of inkjet printing to produce thin film libraries of some PPE-PPV derivatives.[31] PPE-PPV combines the interesting intrinsic properties of both PPE (high absorption coefficients, high electron affinity, and high fluorescence quantum yield in nonaggregated state) and PPV (suitability in the design of devices) into a single polymeric backbone, in addition to novel structure-specific properties.[32]

However, the attachment of alkoxy side chains can also lead to remarkable changes in the optical, electronic, and transport properties of solid state conjugated polymers.[32–34] 4-fold alkoxy-substituted poly(*p*-phenylene-ethynylene)-*alt*-poly(*p*-phenylene-vinylene)s (PPE-PPVs) have tunable optoelectronic properties and thus variable emission color (green to red).[35,36] It has been shown that this is due to cooperative effects of the alkoxy side chain attached to the PPE and PPV segments, $\mathbf{R^1} = OC_nH_{2n+1}$ and $\mathbf{R^2} = OC_{n'}H_{2n'+1}$, respectively (see Figure 1). In the following, we will use the nomenclature ***Pn/n′*** where *n* and *n′* denote the length of the alkoxy side chain attached to the PPE and PPV segments, respectively. Among the first reported compounds ***Pn/n′***, polymer **P18/8** was distinct in its solid state photophysical properties.[37,38] Whereas the other polymers (e.g., **P12/12**, **P18/18**, **P12/18**) were yellow in color and exhibited well-structured emission spectra and high fluorescence quantum yields, **P18/8** was orange-red in color and was characterized with a broad, less-structured, and red-shifted emission spectrum as well as lower fluorescence quantum yield, indicative of strong $\pi-\pi$ interactions.[32,39] To gain insight into the peculiarity of **P18/8**, we required a systematic investigation of the cooperative effects of the length of the side chain attached on the PPE and PPV segments. For this purpose, two series of polymers ***Pn/n′*** were synthesized and characterized.

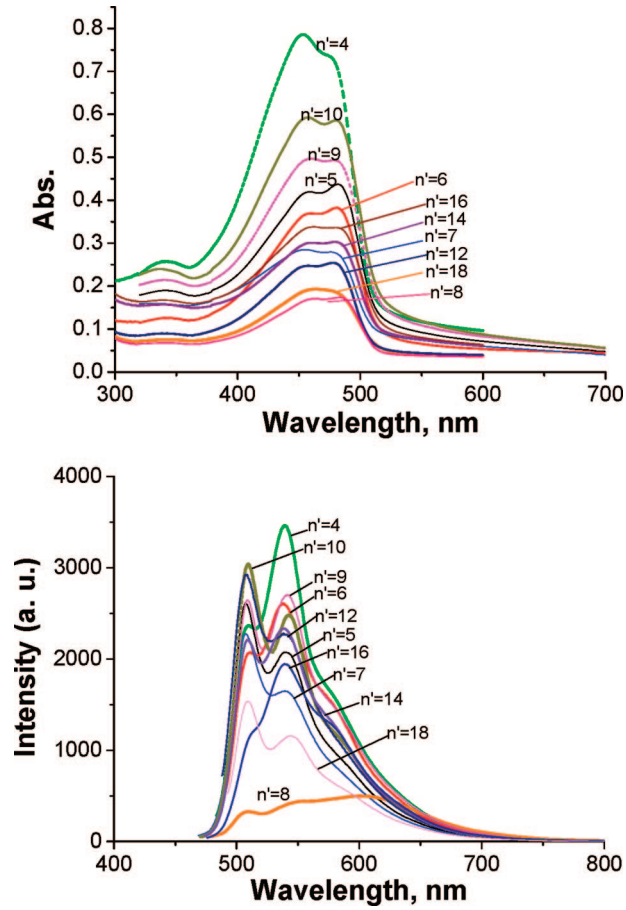

Figure 2. Absorption and photoluminescence spectra of the ***P18/n′*** ($n' = 4-18$) polymers films.

In the first series, $\mathbf{R^1} = OC_{18}H_{37}$ was kept constant and $\mathbf{R^2} = OC_{n'}H_{2n'+1}$ was varied with $\boldsymbol{n'} = 4-10, 12, 14, 16, 18$).[40] Figure 2 shows the absorption and emission spectra of the polymers. Except for **P18/8**, all the polymers ***P18/n′*** exhibit well-structured and intense emission spectra and a yellow color in the solid state.

(24) Haskal, E. I.; Büchel, M.; Duineveld, P. C.; Sempel, A.; van de Weijer, P. *MRS Bull.* **2002**, *27*, 864.
(25) Chang, B. S.-C.; Liu, J.; Bharathan, J.; Yang, Y.; Onohara, J.; Kido, J. *Adv. Mater.* **1999**, *11*, 734.
(26) Shimoda, T.; Morii, K.; Seki, S.; Kiguchi, H. *MRS Bulletin* **2003**, *28*, 821.
(27) de Gans, B.-J.; Duineveld, P. C.; Schubert, U. S. *Adv. Mater.* **2004**, *16*, 204.
(28) Tekin, E.; de Gans, B.-J.; Schubert, U. S. *J. Mater. Chem.* **2004**, *14*, 2627.
(29) Yoshioka, Y.; Calvert, P. D.; Jabbour, G. E. *Macromol. Rapid Commun.* **2005**, *26*, 238.
(30) Wang, J.; Mohebi, M. M.; Evans, J. R. G. *Macromol. Rapid Commun.* **2005**, *26*, 304.
(31) Tekin, E.; Wijlaars, H.; Holder, E.; Egbe, D. A. M.; Schubert, U. S. *J. Mater. Chem.* **2006**, *16*, 4294.
(32) Egbe, D. A. M.; Roll, C. P.; Birckner, E.; Grummt, U.-W.; Stockmann, R.; Klemm, E. *Macromolecules* **2002**, *35*, 3825.
(33) Egbe, D. A. M.; Bader, C.; Nowotny, J.; Gunther, W.; Klemm, E. *Macromolecules* **2003**, *36*, 5459.
(34) Egbe, D. A. M.; Bader, C.; Klemm, E.; Ding, L.; Karasz, F. E.; Grummt, U.-W.; Birckner, E. *Macromolecules* **2003**, *36*, 9303.
(35) Egbe, D. A. M.; Tillmann, H.; Birckner, E.; Klemm, E. *Macromol. Chem. Phys.* **2001**, *202*, 2712.
(36) Ding, L.; Lu, Z.; Egbe, D. A. M.; Karasz, F. E. *Macromolecules* **2004**, *37*, 10031.
(37) Egbe, D. A. M.; Ulbricht, C.; Orgis, T.; Carbonnier, B.; Kietzke, T.; Peip, M.; Metzner, M.; Gericke, M.; Birckner, E.; Pakula, T.; Neher, D.; Grummt, U.-W. *Chem. Mater.* **2005**, *17*, 6022.
(38) Carbonnier, B.; Egbe, D. A. M.; Birckner, E.; Grummt, U.-W.; Pakula, T. *Macromolecules* **2005**, *38*, 7546.
(39) Egbe, D. A. M.; Roll, C. P.; Klemm, E. *Des. Monomers Polym.* **2002**, *5*, 245.
(40) Carbonnier, B.; Pakula, T.; Egbe, D. A. M. *J. Mater. Chem.* **2005**, *15*, 880.

In the second series **P(*n′*+10)/*n′*** (with ***n′*** = 6−9), the difference of 10 methylene units between $\mathbf{R^1}$ and $\mathbf{R^2}$ was kept constant as in **P18/8**.[37] It was found that bulk samples of the polymers bearing an even number of carbons, i.e., **P16/6** and **P18/8**, were orange-red in color, whereas their odd-numbered counterparts **P17/7** and **P19/9** were yellow. Despite the similarity of bulk color, **P16/6** (λ_a = 458, 482 nm, λ_f = 556, Φ_f = 65%) and **P18/8** (λ_a = 456 nm, λ_f = 614, Φ_f = 24%) show differences in the thin film emissive behavior.[37] Here, λ_a and λ_f denote the absorption and fluorescence wavelengths and Φ_f the fluorescence quantum yield.

In this contribution, we present the third series of polymers denoted as **P*n*/8** with the goal to further elucidate the special photophysical properties of **P18/8**. This time, $\mathbf{R^2}$ = octyloxy (*n′* = 8) was kept constant and the length of $\mathbf{R^1} = OC_nH_{2n+1}$ was varied (*n* = 12−19). Subsequently, the resulting polymers were successfully processed via inkjet printing into thin films. The absorption and photoluminescence spectra as well as the relative and absolute fluorescence quantum yields of the polymers in solution and in the solid state have been measured. Furthermore, differential scanning calorimetry (DSC) measurements of the polymers as well as nanoindentation of their inkjet printed thin films were performed to better understand the differences in the photophysical properties with respect to the length of the side chains at $\mathbf{R^1}$. Finally, PLEDs with the device architecture ITO//PEDOT:PSS//**P*n*/8**//Ca//Ag have been fabricated using spin-coating and inkjet printing, and the performance of both types were tested.

Experimental Section

Polymer Synthesis. *Poly[1,4-phenylenethynylene-1,4-(2,5-dihexadecyloxyphenylene)-1,4-phenylenethene-1,2-diyl-1,4-(2,5-dioctyloxyphenylene)ethene-1,2-diyl] (**P16/8**).* 1,4-Bis(4-formylphenylethynyl)-2,5-dihexadecyloxybenzene (**1**−**16**) (813 mg, 0.62 mmol) and 2,5-dioctyloxy-*p*-xylylene-bis(diethylphosphonate) (**2**) (635 mg, 0.62 mmol) were dissolved in dried toluene (50 mL) while stirring vigorously under argon and heating under reflux. The polycondensation started by adding potassium *tert*-butoxide (415 mg, 3.7 mmol). In spite of the rapidly increasing viscosity, the reaction solution was held mixable by adding further dried toluene in small portion ($\Sigma \approx 3$ mL) over the time of the reaction. After 15 min, benzaldehyde (0.4 mL, 0.42 g, 4 mmol) was added. Toluene (40 mL) and an excess of dilute HCl were added 2 min later. The organic layer was separated and extracted several times with distilled water until the water phase became neutral (pH 6−7). A Dean–Stark apparatus was used to dry the organic layer. The hot (50–60 °C) toluene solution was filtered; the filtrate was concentrated to the minimum by using a rotary evaporator and then precipitated in vigorously stirred methanol (300 mL). The polymer was extracted 12 h with methanol, dissolved once more in a small amount of toluene, and reprecipitated in methanol. 96 mg (0.0884 mmol, pertaining of the repeating unit) of orange red polymer were obtained. IR: 3052 (w, $-C_{aryl}-H$), 2920 and 2850 (vs, $-CH_2-$ and CH_3-), 2202 (w, disubst. $-C\equiv C-$), 1606 (w,$-CH=CH-$), 1218 (s, $C_{aryl}-$ OR), 974 (m, trans $-CH=CH-$) cm^{-1}. Anal. Calcd for $(C_{80}H_{116}O_4)_n$ ($(1141.80)_n$): C, 84.15; H, 10.24. Found: C, 82.45; H, 9.93. ^{1}H NMR (400 MHz, CD_2Cl_2, 298 K): δ 0.79–0.99 ($-CH_3$), 1.09–1.70 ($-(CH_2)_5-$ and $-(CH_2)_{13}-$), 1.80–1.99 ($-O-CH_2-CH_2-$), 3.95–4.20 ($-O-CH_2-$), 6.98–7.75 (aromatic and vinylene H′s). ^{13}C NMR (75.5 MHz, CD_2Cl_2, 298 K): δ 13.95 ($-CH_3$), 22.26, 26.68, 25.89, 28.92, 28.96, 29.01, 29.08, 29.26, 29.31, 31.43 31.51 ($-(CH_2)_6-$, $-(CH_2)_{14}-$), 69.08, 69.22 ($-CH_2-O-$), 86.59 ($-C\equiv C_4-$), 94.65 ($-C_5\equiv C-$), 110.04 ($C_{aryl,14}-H$), 113.52 ($-C_{aryl,3}-C.$), 116.33 ($C_{aryl,2}-H$), 124.27 ($C_{aryl,12}$), 126.00, 126.34 ($-C_{10}=C_{11}-$), 127.53 ($C_{aryl,6}-C.$), 131.37 ($C_{aryl,7,8}$), 137.64 ($C_{aryl,9}-C=$), 151.79 ($C_{aryl,13}-OR_2$), 153.22 ($C_{aryl,1}-OR_1$).

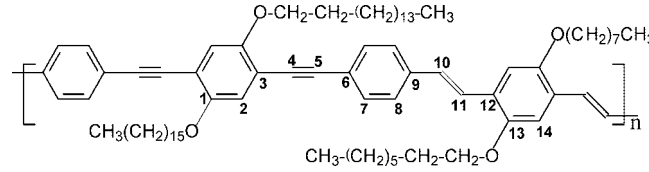

*Poly[1,4-phenylenethynylene-1,4-(2,5-didodecyloxyphenylene)-1,4-phenylenethene-1,2-diyl-1,4-(2,5-dioctyloxyphenylene)ethene-1,2-diyl] (**P12/8**).* Anal. Calcd for $(C_{72}H_{100}O_4)_n$ ($(1029.58)_n$): C, 83.99; H, 9.79. Found: C, 84.41; H, 10.08.

*Poly[1,4-phenylenethynylene-1,4-(2,5-ditridecyloxyphenylene)-1,4-phenylenethene-1,2-diyl-1,4-(2,5-dioctyloxyphenylene)ethene-1,2-diyl] (**P13/8**).* Anal. Calcd for $(C_{74}H_{104}O_4)_n$ ($(1057.64)_n$): C, 84.04; H, 9.91. Found: C, 81.23; H, 10.05.

*Poly[1,4-phenylenethynylene-1,4-(2,5-ditetradecyloxyphenylene)-1,4-phenylenethene-1,2-diyl-1,4-(2,5-dioctyloxyphenylene)ethene-1,2-diyl] (**P14/8**).* Anal. Calcd for $(C_{76}H_{108}O_4)_n$ ($(1085.69)_n$): C, 84.08; H, 10.03. Found: C, 83.17; H, 9.72.

*Poly[1,4-phenylenethynylene-1,4-(2,5-dipentadecyloxyphenylene)-1,4-phenylenethene-1,2-diyl-1,4-(2,5-dioctyloxyphenylene)ethene-1,2-diyl] (**P15/8**).* Anal. Calcd for $(C_{78}H_{112}O_4)_n$ ($(1113.74)_n$): C, 84.12; H, 10.14. Found: C, 83.37; H, 10.37.

*Poly[1,4-phenylenethynylene-1,4-(2,5-diheptadecyloxyphenylene)-1,4-phenylenethene-1,2-diyl-1,4-(2,5-dioctyloxyphenylene)ethene-1,2-diyl] (**P17/8**).* Anal. Calcd for $(C_{82}H_{120}O_4)_n$ ($(1169.85)_n$): C, 84.19; H, 10.34. Found: C, 83.68; H, 10.32.

*Poly[1,4-phenylenethynylene-1,4-(2,5-dioctadecyloxyphenylene)-1,4-phenylenethene-1,2-diyl-1,4-(2,5-dioctyloxyphenylene)ethene-1,2-diyl] (**P18/8**).* Anal. Calcd for $(C_{84}H_{124}O_4)_n$ ($(1197.90)_n$): C, 84.22; H, 10.43. Found: C, 83.40; H, 10.45.

*Poly[1,4-phenylenethynylene-1,4-(2,5-dinonadecyloxyphenylene)-1,4-phenylenethene-1,2-diyl-1,4-(2,5-dioctyloxyphenylene)ethene-1,2-diyl] (**P19/8**).* Anal. Calcd for $(C_{86}H_{128}O_4)_n$ ($(1225.95)_n$): C, 84.26; H, 10.52. Found: C, 84.07; H, 10.67.

Structure Characterization. ^{1}H NMR and ^{13}C NMR spectra have been recorded on a Mercury 400 MHz and a Gemini 300 MHz spectrometer (Varian) at 298 K in deuterated methylene chloride (CD_2Cl_2). Elemental analysis (EA) was carried out on an EuroEA3000 elemental analyzer (EuroVector) for the elements C, H, N and S. Infrared (IR) spectra were recorded using a Tensor 37 RT (Bruker) with a grazing angle setup. Gel permeation chromatography (GPC) was performed with a Shimadzu system equipped with a SCL-10AV vp system controller. THF was used as eluent at a flow rate of 1 mL/min. The molecular weights were calculated against polystyrene standards.

Differential Scanning Calorimetry. DSC measurements were carried out on a Mettler DSC 30 with a cell purged with nitrogen. Samples of approximately 10 mg were used. Calibration for temperature and enthalpy changes was performed using an indium standard. The temperature was changed with a rate of 10 K/min covering a temperature range between 293 and 493 K. Data analysis was performed on the first cooling and second heating runs which are considered to reflect the properties of

Scheme 1. Schematic Representation of the Repeating Unit of Polymer P16/8

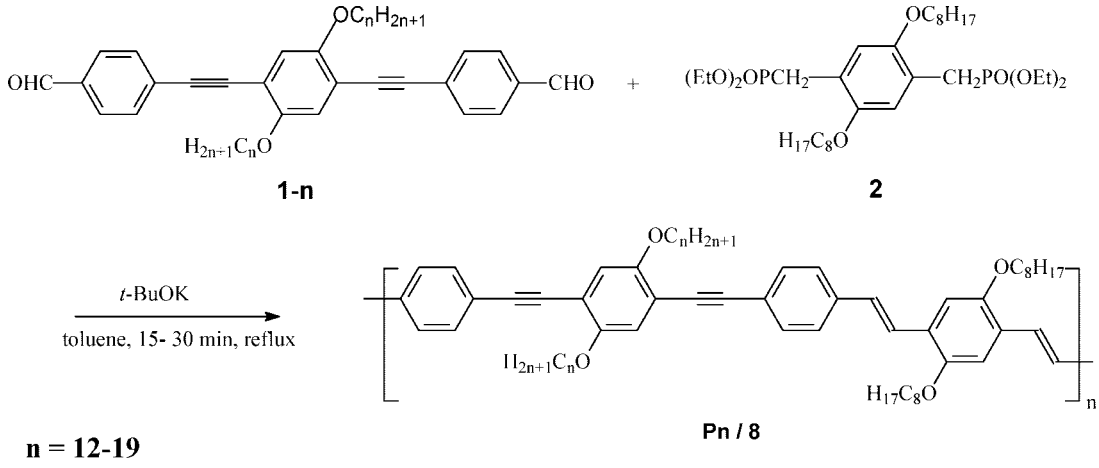

the compact bulk material. Transition temperatures were determined from the peak maxima.

Inkjet Printing. For the preparation of the inkjet-printed films an Autodrop System (Microdrop Technologies, Norderstedt, Germany) was used. Thin films of approximately 80 nm thickness were printed from toluene/*o*-dichlorobenzene (90/10 $^{v}/_{v}$) on glass substrates for quantum yields measurements and on ITO-coated glass substrates for device fabrication. Stable droplets were obtained with a pulse height of 75 V and a pulse width of 45 μs. Thick films (1−5 μm) for nanoindentation measurements were also prepared by inkjet printing. The thicknesses of the polymer films were measured using an optical profilometer (Fogale Zoomsurf, France).

Nanoindentation. Depth-sensing indentation was performed using a Hysitron TriboIndenter, equipped with a 2D transducer and a Berkovich tip. Frame compliance and tip area function calibration (for a contact depth range between 27 and 186 nm) were performed on fused quartz. The glass slides with PPE-PPV films were fixed by vacuum to the TriboIndenter sample holder plate, to avoid extra frame compliance. The PPE-PPV films were indented employing the following load function: 5 s loading to maximum load, 5 s hold time at maximum load, and 0.5 s unloading. In three distinct regions of each PPE-PPV surface, six indents were made with a maximum load that was varied from 65 to 15 μN in steps of 10 μN. The first two measurements on each region, i.e., all the indents performed employing maximum loads levels of 65 and 55 μN, were disregarded, as these experiments may be affected by some thermal drift. In addition, the indentation contact depth at these load levels often exceeded the tip area function calibration range. From the load-displacement responses, the reduced modulus was obtained using the Oliver and Pharr procedure, with $\beta = 1$ and $\epsilon = 0.75$, which was subsequently converted into the indentation modulus E_i assuming a Poisson ratio of 0.4.[41] Usually the modulus obtained by indentation somewhat overestimates the Young's modulus.[42]

If the average E_i obtained in a certain region was significantly larger than the values obtained elsewhere on the same PPE-PPV surface, and E_i showed in that region an increase with increasing employed maximum load level, the results were most likely influenced by the stiffness of the subjacent substrate and were therefore discarded. Visual inspection indeed revealed local variation in the thickness of the printed film.

Table 1. Data from GPC, Yields, and the Bulk Color of the Polymers

code	M_n (g/mol)	PDI	DP	yield (%)	bulk color
P12/8	20 500	5.2	20	26	yellow
P13/8	19 050	2.9	18	50	yellow
P14/8	42 600	6.0	39	50	yellow
P15/8	27 100	3.1	24	52	yellow
P16/8	21 800	2.4	19	60	orange
P17/8	27 700	2.8	24	20	orange
P18/8	11 060	3.0	10	60	orange
P19/8	31 800	2.9	26	50	orange

Photophysical Characterization. The absorption spectra were recorded in dilute chloroform solution (1×10^{-5} to 1×10^{-6} M) on an UV/vis-NIR spectrometer Lambda 19 purchased from Perkin-Elmer. Quantum corrected emission spectra were measured in dilute chloroform solution (1×10^{-6} M) with a LS 50 luminescence spectrometer (Perkin-Elmer). The fluorescence quantum yields were calculated relative to quinine sulfate ($\Phi_f = 55\%$). The absorbance at the excitation wavelength was kept below 0.05 for the samples and the reference.[32]

A UV–vis/fluorescence plate reader (Flashscan 530) from Analytik Jena (Jena, Germany) was used to measure the respective fluorescence spectra of the printed PPE-PPV films. The emission spectra and absolute quantum yields of the thin films were measured on a Hamamatsu C9920–02 system and a homemade setup. The absolute photoluminescence quantum yields of thin films of conjugated polymers using homemade setup, has been determined according the methods of De Mello et al.[43] and Palsson Monkman[44] with an integrating sphere inserted in the fluorescence spectrometer CD900FS (Edinburgh Analytical Instruments). A custom designed integrating sphere (model 05–105, AMKO) with an inner diameter of 105 mm was used coated inside with $BaSO_4$. The excitation was made with a tungsten lamp of variable intensity in order to obtain suitable conditions to measure the fluorescence of the sample and the scattered excitation light with the same slit widths of the spectrometer.

PLED Fabrication and Characterization. The concentrations of the utilized solutions for inkjet printing and spin-coating were 4 and 8.5 mg/mL, respectively. Spin-coating took place under a nitrogen atmosphere, whereas the preparation of the active layers by inkjet printing did not occur under inert conditions. Therefore, water condensation on the film surface cannot be excluded. The cathode, consisting of a 4 nm thin layer of Ca and an Ag layer

(41) Oliver, W. C.; Pharr, G. M. *J. Mater. Res,* **1992**, *7*, 1564.
(42) Tranchida, D.; Piccarolo, S.; Loos, J.; Alexeev, A. *Macromolecules* **2007**, *40*, 1259.
(43) de Mello, J. C.; Wittmann, H. F.; Friend, R. H. *Adv. Mater.* **1997**, *14*, 757.
(44) Palsson, L.-O.; Monkman, A. P. *Adv. Mater.* **2002**, *9*, 230.

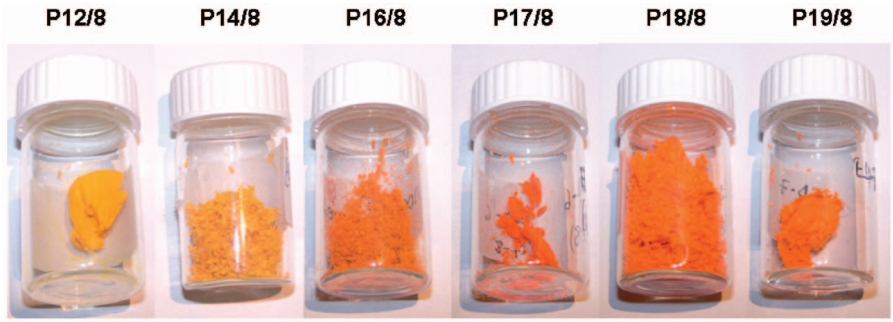

Figure 3. Photographs of the polymer bulk materials.

(150 nm), was deposited by thermal evaporation at a base pressure of 1×10^{-6} mbar. The device characterization was done with a Keithley 2400 source meter, a calibrated photodiode and an Ocean Optics SD2000 CCD spectrometer under an argon atmosphere.

Results and Discussion

Synthesis and Characterization. The polymers **P*n*/8** were obtained via Horner-Wadsworth-Emmons olefination reaction of 1,4-bis-(4-formylphenylethynyl)-2,5-dialkoxybenzene (**1**−***n***) and 2,5-dioctyloxy-*p*-xylylene-bis(diethylphosphonate) (**2**) based on a synthetic protocol described elsewhere (Scheme 1).[32–35,37] The reaction time was kept below 30 min in order to avoid insoluble products.[37] GPC results (number-average molecular weight, M_n, polydispersity index, PDI, and degree of polymerization, DP), the yield and the color of the resulting products are summarized in Table 1.

The synthesized polymers exhibit M_n values between 11,000 and 43,000 g/mol (DP ∼10–40) and polydispersity indexes between 2 and 6, as expected from this type of polycondensation reaction.[33] The polymers **P12/8**, **P13/8**, **P14/8** and **P15/8** are yellow in color while the polymers with longer side chains **(n ≥ 16)** are orange. Images of the selected polymers are shown in Figure 3. The polymers **Pn/8** with $n \geq 16$ exhibit better solubility compared to the ones with shorter side chains. This improved solubility makes them more suitable for inkjet printing. Polymers with short side chains occasionally caused nozzle clogging during printing.

Thermal Behavior of the Polymers. The thermotropic mesophase formation for PPE-PPV samples with alkoxy groups of different lengths attached to the PPE segments was investigated using differential scanning calorimetry. The results are compared to previous results obtained on samples where the length of the alkoxy group attached to the PPV was changed ($n' = 4$–16) but n was kept fixed to 18.[40] The DSC thermograms presented in Figure 4 show the data obtained during the first cooling (top) and second heating circle (bottom). The cooling runs reveal that the samples undergo an exothermic transition in a temperature range between 350 and 390 K. The transition temperatures obtained from the peak positions are summarized in Table 2.

The samples with $n = 12$, 13, 16−18 show pronounced peaks most likely due to an isotropic−mesophase transition. This is supported by additional investigations with polarized microscopy performed on the **P18/*n′*** system.[40] The peaks for the samples $n = 16$−18 are rather sharp but the samples $n = 12$ and 13 exhibit highly asymmetric peaks with a rather

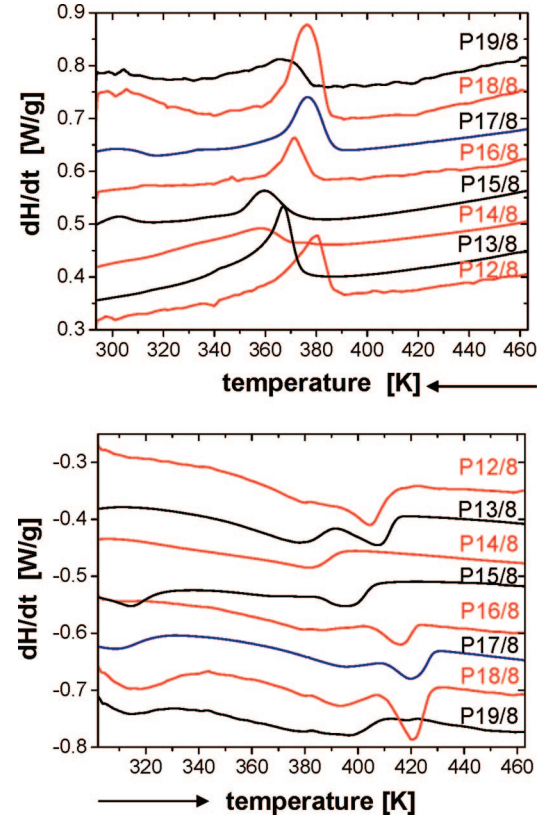

Figure 4. DSC thermograms recorded for the samples **P*n*/8** ($n = 12$−19) during first cooling (top) and second heating run (bottom) with a rate of 10 K/min. Data are vertically shifted for better visualization.

Table 2. Transition Temperatures Obtained from the Peak Positions in the First Cooling and Second Heating Run

	transition temperature (K)		
sample	1st cooling run	2nd heating run	
P12/8	380	404	380
P13/8	367	408	378
P14/8	358		382
P15/8	360		396
P16/8	371	416	387
P17/8	376	420	395
P18/8	376	420	383
P19/8	366		396

extended tail on the low temperature side. The disorder–order transitions in the samples $n = 14$, 15, and 19 are much less pronounced and in comparison to the other samples systematically shifted ($\Delta T \approx 20$ K) to lower temperatures. In analogy to previous results obtained for **P18/*n′*** where the length of the alkoxy chains attached to the phenylene rings in the PPV units was varied,[40] we can conclude that the

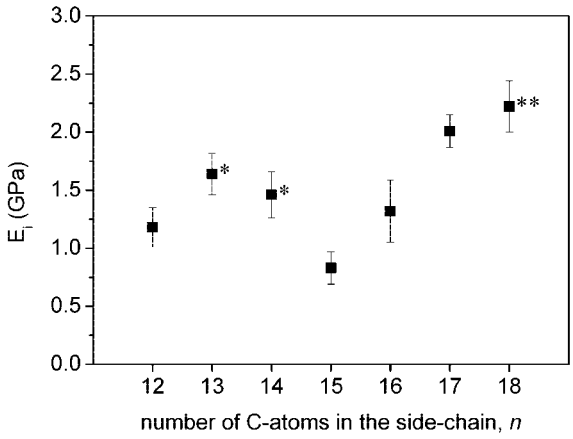

Figure 5. Material stiffness as a function of number of carbon atoms n in the side chain attached to the PPE; * the stiffness may be slightly overestimated because of the small film thickness; ** value based on only one region on the sample surface (other film regions were too thin).

disorder–order phenomenon is strongly connected to the length of the alkoxy group attached to the PPE units (**P*n*/8**). The samples with $n > 15$ show an additional peak at temperature around 320 K, respectively. The peak is exothermic in the cooling and endothermic in the heating run. In accordance with results obtained for alkyl-substituted semiflexible[45] and rigid[46] polymers, this cold transition is most likely due to side chain crystallization.

In the heating runs, the endothermic peaks of the order–disorder transition are systematically shifted to higher temperatures ($\Delta T \approx 35$ K) compared to the exothermic peaks observed in the cooling runs. The heating runs clearly reveal a two-step order–disorder transition separated by about $\Delta T \approx 30$ K for the samples with $n = 12, 13, 16-18$. Those samples showed a pronounced peak at the crystallization transition in the cooling run. The samples ($n = 14, 15, 19$) with less-pronounced peaks in the cooling run exhibit a single-step order–disorder transition in the heating run. The transition temperatures of these transitions correspond to the lower temperature transition observed for the samples with $n = 12, 13, 16-18$.

In conclusion, the mesophase formation is strongly connected to the length of the alkoxy groups attached to the phenylene rings in the PPE units. For some of the samples we observed a two-step transition. There is no clear evidence that longer alkoxy groups are advantageous for mesophase formation. However, samples with $n > 15$ show an additional transition around 320 K most likely due to side chain crystallization.

Nanoindentation Experiments. To obtain moduli that properly reflect the stiffness relevant for future applications, we performed the indentation experiments on inkjet printed films, as inkjet printing is the most probable processing route for future application of these materials.

If the films are thin, the indenter also partially probes the stiffness of the underlying substrate. For some of the films, marked in Figure 5 by an asterisk, this substrate effect may, even after specific data handling (described in the Experimental Section), result in a small (<10%) overestimation of the material stiffness. It should be noted that measurement on the **P19/8** was not performed because of the inhomogeneous layer thickness.

Table 3. Absorption and Emission Data of the Polymers in Dilute Chloroform Solutions

code	λ_a (nm)	E_g^{opt} (eV)	λ_f[a] (nm)	I_{0-1}/I_{0-0}	$\Phi_{f,rel.}$ (%)
P12/8	448	2.54	489, 520	0.52	70
P13/8	448	2.54	489, 520	0.52	71
P14/8	448	2.54	489, 520	0.50	74
P15/8	448	2.54	489, 520	0.53	68
P16/8	448	2.53	489, 520	0.52	62
P17/8	448	2.53	489, 520	0.56	70
P18/8	448	2.54	490, 520	0.55	74 (70)[b]
P19/8	448	2.54	490, 520	0.60	70

[a] Underlined values belong to the main peaks. [b] Absolute Φ_f measured by Hamamatsu PL System.

In Figure 5, the measured elastic moduli are plotted versus the length of the side chains attached to the PPE units. The results suggest a small increase of material stiffness with increasing n above 16. In previous publications on PPE-PPVs, the spatial arrangement of the alkoxy side-chains and the conjugated backbones was studied by atomic force microscopy (AFM) and wide-angle X-ray scattering (WAXS).[38] It was shown that the aromatic rings in the backbone of neighboring molecules align, and that the alkoxy side-chains form "interlayers" between these stacks of aromatic rings.[38] We expect high stiffness for the stacks of aligned aromatic rings, whereas the amorphous interlayers of alkoxy side chains should possess a lower stiffness. Thus, one would expect a decrease in stiffness with increasing soft interlayer dimension, i.e., with increasing alkoxy side-chain length. However, this is not observed (see Figure 5). On the contrary, the results suggest a small increase of material stiffness with increasing n. This might be taken as an indication that the degree of stacking of the aromatic rings increases for longer alkoxy side chains attached to the PPE units thus causes a stiffening of the main chain layers. Alternatively, DSC experiments reveal crystallinity of the side-chain interlayers for samples with $n \geq 16$. Side-chain organization would increase the interlayer stiffness. Hence, most likely the increase in sample stiffness is due to side-chain crystallization.

Photophysical Investigations. The photophysical data of the polymers **Pn/8** shown in Table 3 are determined in dilute chloroform solutions. The results comprise the wavelength at the absorption and emission maximum, λ_a and λ_f, the optical band gap energy, E_g^{opt},[33] and the relative fluorescence quantum yield, Φ_f. The corresponding absorption and emission spectra are shown in Figure 6. Regardless of n, and as expected,[37] all the polymers show similar photophysical behavior in dilute chloroform solution. Their main absorption band is located at 448 nm ($E_g^{opt} = 2.54$ eV). The fluorescence spectra show their maximum at 490 nm and a shoulder at 520 nm. A slight increase of the intensity ratio (I_{0-1}/I_{0-0}) of the shoulder band intensity (I_{0-1}) to the intensity at the maximum (I_{0-0}) is observed with increasing n, which is probably caused by different deviations from the strict

(45) Lee, J. L.; Pearce, E. M.; Kwei, T. K. *Macromolecules* **2001**, *34*, 1570.
(46) Huang, W. Y.; Gao, W.; Kwei, T. K.; Okamoto, Y. *Macromolecules* **1997**, *30*, 6877.

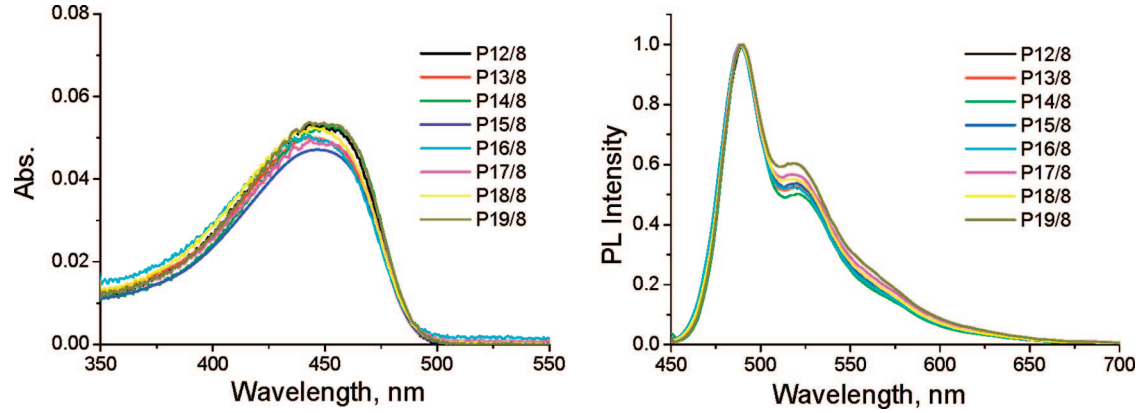

Figure 6. Absorption and photoluminescence spectra of the polymers **P*n*/8** (n = 12−19) in dilute chloroform solutions.

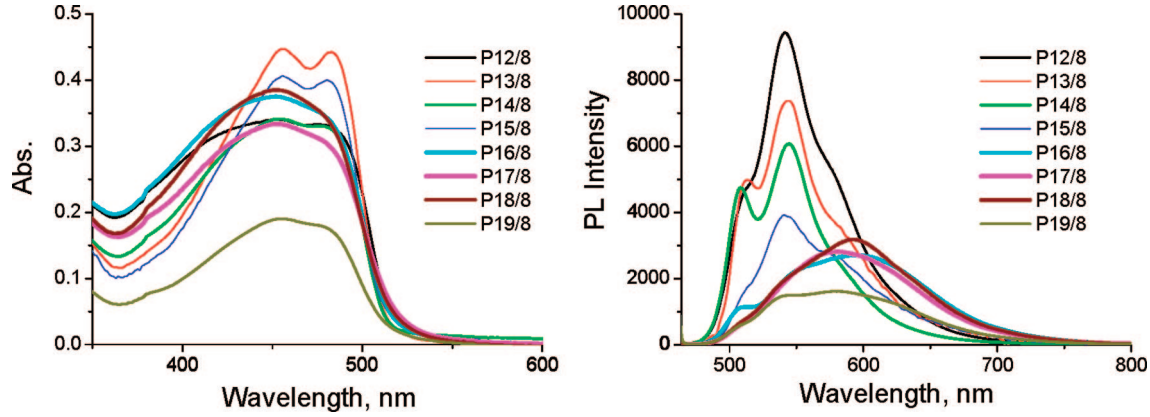

Figure 7. Absorption and the photoluminescence spectra of the polymers **P*n*/8** (n = 12−19) films printed from toluene/*o*-dichlorobenzene (90/10 $^{v}/_{v}$) solutions.

Table 4. Absorption and Emission Data of the Polymers in Thin Films

code	λ_a[a] (nm)	E_g^{opt} (eV)	λ_f[a] (nm)	$\Phi_{f,abs.}$ (%)[b]	$\Phi_{f,abs}$ (%)[c]
P12/8	453, 479	2.38	510, 540, 574	18	16
P13/8	455, 482	2.42	512, 543, 580	18	
P14/8	453, 478	2.42	507, 543	15	10
P15/8	455, 481	2.40	512, 540, 582	17	
P16/8	451	2.40	507, 550, 595	12	12
P17/8	451	2.37	582	14	12
P18/8	450	2.38	533, 593	17	15
P19/8	454, 478	2.38	509, 536, 582	13	17

[a] Underlined values belong to the main peaks. [b] Quantum yields obtained from Hamamatsu. [c] Quantum yields obtained from homemade PL set up.

Table 5. Electroluminescence Data of the Polymers

	spin-coated			inkjet printed	
code	λ_{el} (nm)	efficiency (Cd/A)	V_{ONSET} (V)	efficiency (Cd/A)	V_{ONSET} (V)
P12/8	505, 550 (4 V) 505, 550 (4.5V)	0.29	2.5	0.08	6.6
P14/8	510, 550 (5 V) 510, 550 (7 V) 510, 550 (9 V)	0.12	3.3	0.06	2.8
P16/8	580 (5 V) 550 (6 V) 500 (7 V)	0.03	3.5		
P17/8	600 (8 V) 550 (10 V) 510 (12 V)	0.12	4.6	0.07	8.0
P18/8	590 (6 V) 520 (6.5 V)	0.22	3.5		
P19/8	560 (7 V) 520 (7.5V)	0.24	2.7		

linearity of the polymer backbone due to bending motions.[47] One should note that high relative as well as absolute Φ_f values of approximately 70% were obtained.

The influence of the side-chain length, n, becomes obvious in the solid-state photophysical behavior. Figure 7 presents the absorption and PL spectra of the thin polymer films inkjet printed on glass substrates. Because of the chromophore–chromophore interactions, there is a red-shift of both the absorption and PL spectra in thin films relative to those in solution. Although the main absorption band was around 450 nm for the polymers (**P*n*/8**) with n = 16−18, the absorption band of the polymers with n = 12−15 and 19 consist of two maxima around 450 and 480 nm. The optical band gap values calculated from the absorption spectra are approximately 2.40 eV. Polymers with short side chains (n = 12−15) exhibit relatively narrow PL spectra, whereas the polymers with longer side chains have broad emission spectra and their maximum emission wavelengths are approximately 50 nm red-shifted (see Figure 7, Table 4). Absolute fluorescence quantum yields of the thin films are lower than those in solution because of enhanced intermolecular interactions. Absolute Φ_f measurements using two different experimental setup exhibited comparable values.

(47) Westenhoff, S.; Beenken, W. J. D.; Yartsev, A.; Greenham, N. C. *J. Chem. Phys.* **2006**, *125*, 154903.

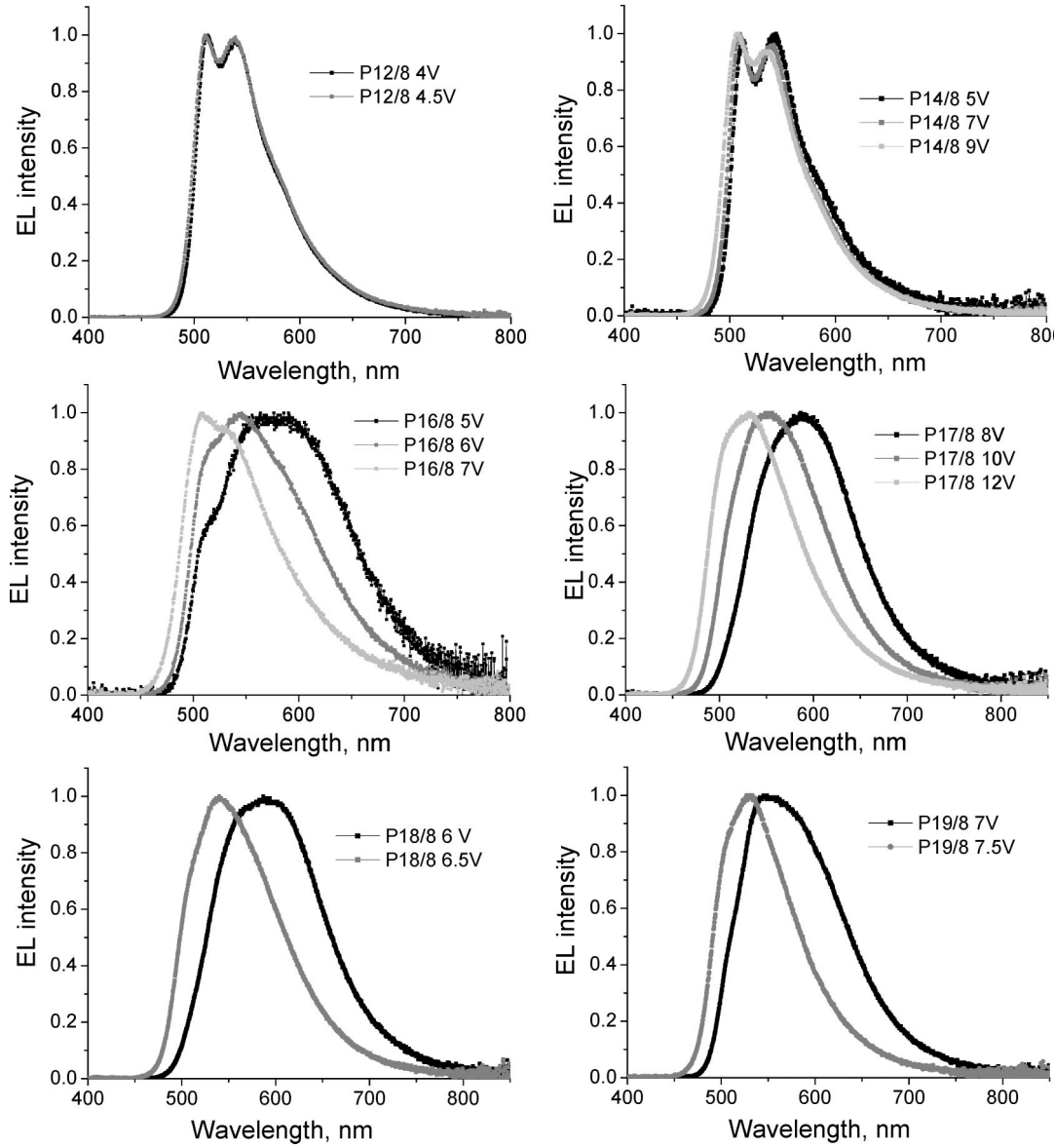

Figure 8. Electroluminescence spectra of the polymers measured at various voltages.

The visual impression of the bulk polymers (Figure 3) reflects the differences in the emission spectra. Longer side chains attached to the PPE units seem to support better packing of the conjugated backbones, which results in red shift of the emission spectra due to increased $\pi-\pi$ stacking and excimer emission.[36,48,49]

Electroluminescence Investigations. Single layer PLEDs with ITO//PEDOT:PSS//**P*n*/8** (~80 nm)//Ca(4 nm)//Ag(150 nm) were fabricated and characterized. The active layers were prepared using both spin-coating and inkjet printing from toluene/o-dichlorobenzene (90/10 $^{v}/_{v}$) solutions. Performance parameters of devices of selected polymers are summarized in Table 5. The best device performance was obtained with a spin-coated active layer of polymer **P12/8** yielding a power efficiency of 0.29 Cd/A. The spin-coated devices with **P18/8** and **P19/8** as active layers also exhibited relatively good device performances with power efficiencies of 0.22 and 0.24 Cd/A, respectively. No correlation between the side-chain length and the LED efficiencies has been observed. All devices exhibited low onset voltages in the range of 2.5 up to 4.6 V. Devices with inkjet printed active layers revealed only poor performances, i.e., low efficiencies and higher onset voltages. This may be due to the inhomogeneous thicknesses of the inkjet printed PPE-PPV active layers. Because the preparation of the inkjet printed layers took place in ambient conditions instead of inert conditions, possible water condensation on the deposited surfaces could also affect the performances.

Electroluminescence spectra of the devices with **P*n*/8** active layers are shown in Figure 8. The shape of the spectra and wavelength of the EL maximum depend on the alkoxy side chain length. The polymers **P12/8** and **P14/8** exhibit two well resolved peaks located around 500 and 550 nm. Polymers with longer side chains have broader EL spectra which are red-shifted with maximum intensities located between 550 and 600 nm. Increasing the applied bias voltage

(48) Koo, J. B.; Kima, S. H.; Lee, J. H.; Ku, C. H.; Lima, S. C.; Zyunga, T. *Synth. Met.* **2006**, *156*, 110.
(49) Ding, L.; Egbe, D. A. M.; Karasz, F. E.; *Macromolecules* **2004**, *37*, 6124.

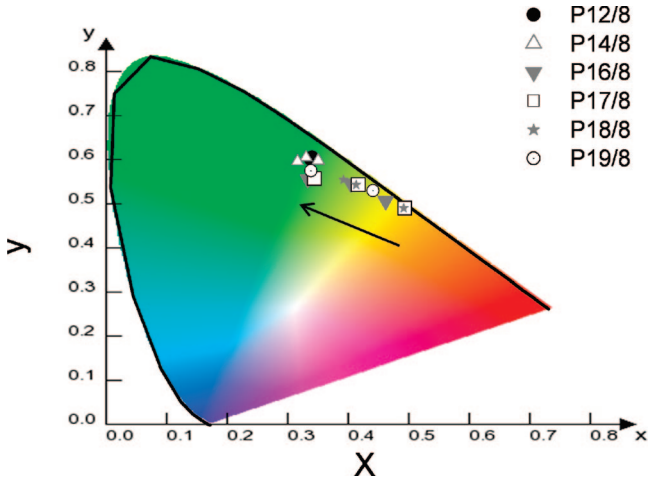

Figure 9. Commission Internationale de l′ Éclairage (CIE) (*x*,*y*) coordinates of all PLEDs. EL colors of the polymers **P*n*/8** (n = 16−19) are shifting from orange or yellow to green with increasing bias voltages. Arrow shows the direction of the color shift for these polymers.

leads to a blue-shift of the EL of the polymers **P*n*/8** (n = 16−19), whereas the EL of the polymers **P12/8** and **P14/8** are stable (see Figure 8 and Table 5). For example, at low bias voltage (5 V) **P16/8** emits orange light at around 580 nm. Increasing the bias voltage to 6 and 7 V led to a blue-shift of the emission of 30 and 80 nm, respectively (see Figure 8). It also changes the shape of the EL spectra of **P16/8** to become comparable to that of **14/8**. The process is irreversible. Application of higher electric fields causes local heating in the polymer film which leads to changes in the conformation of the polymer backbone by uplifting the strong $\pi-\pi$ interactions. Similar results were reported previously.[36,49–52] Therefore the EL spectrum of **P16/8** becomes similar to the EL spectrum of **P14/8**, confirming the literature result that was found for **P18/8**.[37]

In summary, the EL colors of the polymers **P*n*/8** varies from orange to green depending on the side chain as shown in Figure 9. EL colors of the polymers **P*n*/8** (n = 16−19) are not stable and tend to shift from orange or yellow to green with increasing bias voltages.

Conclusions

The effect of the alkoxy side chain attached to the PPE segment on the photophysical properties of the PPE-PPVs has been investigated. The length of the side chains attached to the PPE-segments, C_nH_{2n+1}, has been varied from n = 12−19, whereas the side chains attached to the PPV segments have been kept constant to C_8H_{17}.

Bulk samples with $n < 16$ are yellow, whereas polymers with longer alkoxy side chains $n \geq 16$ are orange. All polymers showed similar absorption and emission spectra in solution. However, even though the absorption spectra of the thin films were comparable, distinct differences were observed for the thin film emission spectra. The thin film emission maxima of the polymers **P*n*/8** with $n \geq 16$ are red-shifted relative to the polymers **P*n*/8** with $n < 16$. Recrystallization of the longer side chains attached to the PPE segment seems to support planarization of the conjugated backbone. This leads for **P*n*/8** with $n \geq 16$ to structures with stronger $\pi-\pi$ interaction, which in turn leads to a red-shift of the emission spectra.

The EL spectra of the polymers show a similar dependency on the side chain length as observed for the PL spectra. Aside of broader and red-shifted EL spectra, **P*n*/8** with longer side chains ($n \geq 16$) revealed a blue-shift of the EL color with increasing bias voltage. This might be ascribed to the reorganization of the chains due to local heating of the active layer.

In conclusion, recrystallization of the longer side chains attached to the PPE segment seems to favor planarization of the conjugated backbone. This leads for **P*n*/*n*′** with $n \geq 16$ to higher organized structures with stronger $\pi-\pi$ interaction, which leads to a red-shift of the emission spectra.

Acknowledgment. This work forms part of the DPI research program (Project 448) and was further supported by NWO and the Fonds der Chemischen Industrie.

CM703312U

(50) Ding, L.; Karasz, F. E.; Lin, Z.; Zheng, M. *Macromolecules* **2001**, *34*, 9183.
(51) Ding, L.; Karasz, F. E.; Lin, Y.; Pang, Y.; Liao, L. *Macromolecules* **2003**, *36*, 7301.
(52) Ding, L.; Karasz, F. E. *J. Appl. Phys.* **2004**, *96*, 2272.